Nanoscale Advances

ROYAL SOCIETY OF CHEMISTRY

PAPER

View Article Online
View Journal | View Issue

Cite this: *Nanoscale Adv.*, 2020, **2**, 3514

Novel star-shaped D–π–D–π–D and $(D–\pi)_2–D–(\pi–D)_2$ anthracene-based hole transporting materials for perovskite solar cells†

Muniyasamy Harikrishnan, Sepperumal Murugesan and Ayyanar Siva *

Three types of novel star-shaped molecular architectures, D–π–D–π–D and $(D–\pi)_2–D–(\pi–D)_2$ anthracene (ANTTPA, AOME, AOHE) based hole transporting materials, are designed for hybrid perovskite solar cells using the Gaussian 09 computation program with the B3LYP/6-31g (d, p) basis set level. The HOMO energy level of the designed materials has a higher HOMO energy level compared to the perovskite HOMO energy level, which is more facile for hole transport from the hole transporting layer to the oxidized perovskite layer. Thereafter, anthracene-based derivatives were synthesized from Buchwald–Hartwig and Mizoroki–Heck cross coupling reactions. The behaviors of the transporting charges were determined by both UV-visible absorbance and emission spectroscopy through solvatochromism experiments. Furthermore, the electrochemical properties also proved that the synthesized compounds had an optimal HOMO energy level in the TiO_2/perovskite/HTM interface. Our hole transport materials (HTMs) have a good film formation compared to the spiro-OMeTAD, which was confirmed from scanning electron microscopy images. The obtained theoretical and experimental data show the suitability of designing anthracene-based derivatives with the potential to be used as hole transporting materials in organic–inorganic hybrid perovskite solar cells.

Received 16th April 2020
Accepted 23rd June 2020

DOI: 10.1039/d0na00299b

rsc.li/nanoscale-advances

1. Introduction

Solar energy is the most promising renewable energy source and the breakthrough research in solar energy is photovoltaics in which organic–inorganic hybrid perovskite solar cells (PSCs) were introduced by Miyasaka *et al.* in 2009.[1] PSCs have attracted immense attention due to the broad light harvesting ranges with direct band gaps, long charge diffusion lengths and high extinction coefficients.[2,3] In PSCs, the hole transporting material (HTM) is the most significant component and plays a crucial role in extracting and transmitting holes from sensitizer materials to the counter electrode. At present, spiro-OMeTAD (2,2-7,7-tetrakis(*N*,*N*′-di-paramethoxy-phenylamine-9,9′-spirobifluorene)) is the HTM material reported to date, and its photo conversion efficiency exceeded up to 20%.[4,5] However, the drawbacks of spiro-OMeTAD are tedious synthetic procedures, less stability, and purification processes having a high demand for commercial applications.[6,7] To date, many researchers have devoted their efforts to finding an organic HTM based on different building blocks, such as tetraphenylethylene,[8] truxene,[9] benzotrithiophene,[10] 3,4-ethylenedioxythiophene,[11] phenothiazine,[12] 1,3,4-oxadiazole,[13] silolothiophene,[14] triazole,[15] furan[16] and so on. F. Zhang *et al.*,[17] reported two HTMs, Z25 and Z26, of which the Z25 HTMs contain 3,4-dimethoxythiophene, which acts as a building block, and 4-methoxy-*N*-(4-methoxyphenyl)-*N*-phenylaniline, which acts as a donor; Z26 HTMs introduce the olefin bond between the building blocks and donor. The olefin bond present in a Z26 HTM has higher hole mobility, higher conductivity, a more homogeneous surface, and also a high PCE compared to that of Z25. But in our case, we changed the 3,4-dimethoxythiophene building blocks with the cheaper starting material of anthracene as a building block. Moreover, anthracene based materials are reported in the various research sectors, such as dye-sensitized solar cells, bulk heterojunction organic solar cells, sensors, and organic light-emitting diode, *etc.*, due to their excellent optical properties, high stability, easily tunable, cost-effectiveness and superior carrier mobility.[18–20] The previously reported HTMs have demerits such as a low light to current efficiency, solubility issues, low stability and high cost. Therefore, the development of a low cost, stable and efficient HTM is a hot research sector. Based on previous research results, we designed anthracene based HTMs and our designed anthracene acts as building block with two types of architecture, D–π–D–π–D and $(D–\pi)_2–D–(\pi–D)_2$ (Fig. 1). In addition to that, we modified the short and long alkyl chains at the terminal ends of the molecule as shown in the Fig. 1. Our intended material energy level parameters were studied by

Supramolecular and Organometallic Chemistry Lab, Department of Inorganic Chemistry, School of Chemistry, Madurai Kamaraj University, Madurai-21, India. E-mail: drasiva@gmail.com; siva.chem@mkuniversity.org

† Electronic supplementary information (ESI) available. See DOI: 10.1039/d0na00299b

density functional theory, after which our designed materials were synthesized in a laboratory scale batch. The main advantages of our synthesized HTMs are that the building blocks of anthracene are an easily available, cost effective material compared to the spiro building blocks; in addition to that, the synthesis of our materials does not need very cold conditions, as spiro-OMeTAD synthesis does (*i.e.* −70 °C). Furthermore, our HTMs have excellent optical and electrochemical properties compared to those of spiro-OMeTAD. The HOMO energy levels of our HTMs are very low when compared to the HOMO energy level of spiro-OMeTAD (−5.02 eV)[12] and match well with that of the perovskite energy level (−5.44 eV). The solubility of our HTMs plays a crucial role in the device making process, our HTMs have a good film forming capacity compared to that of the spiro-OMeTAD because more π-conjugation is present in our material. To the best of our knowledge, this type of molecular architecture helps to increase the PCE of hybrid perovskite solar cells.

2. Experimental section

2.1. Materials

All starting materials and reagents were purchased from Alfa Aesar and Sigma Aldrich, and used as received without further purification. The Mizoroki–Heck coupling reaction was carried out under the protection of nitrogen atmospheric conditions. Silica gel-G plates (Merck) were used for Thin-Layer Chromatography (TLC) analysis with a mixture of petroleum ether and ethyl acetate as the eluent.

2.2. Instruments

^{1}H and ^{13}C NMR spectra were recorded on a Bruker (Avance) 300 MHz and 400 MHz NMR instrument and the chemical shifts were recorded as δ values in parts per million (ppm) relative to tetramethylsilane with coupling constant (J) values in hertz (Hz). The UV-visible absorbance of the prepared materials was examined on a JASCO V-630 UV-Vis spectrophotometer using

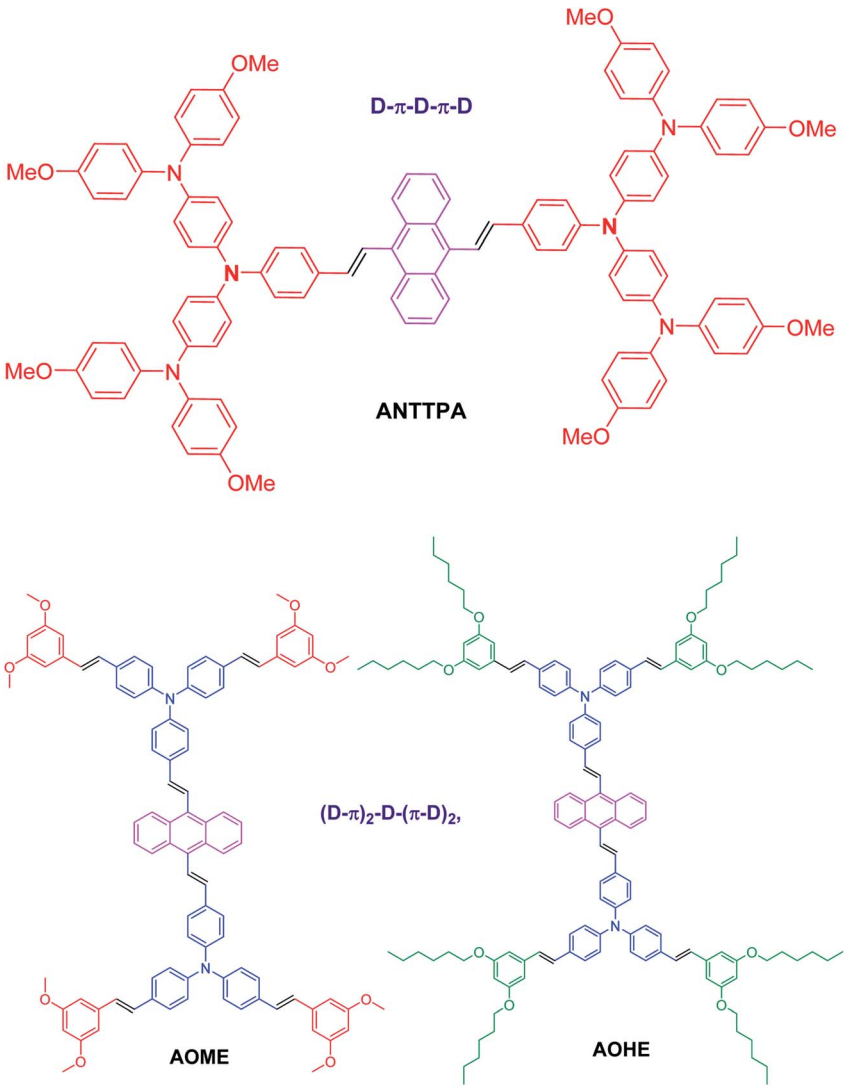

Fig. 1 Molecular structure of the anthracene based HTMs.

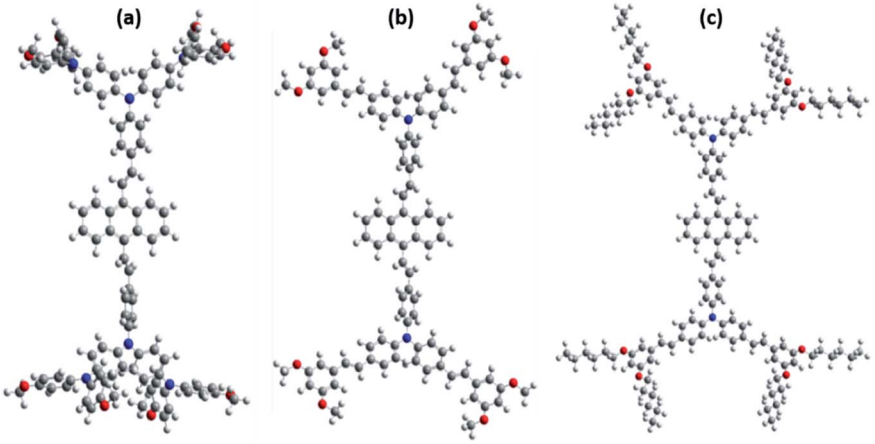

Fig. 2 Optimized structure of the anthracene based HTMs (a) ANTTPA, (b) AOME, and (c) AOHE.

a quartz cuvette with a 1 cm path length. The excitation and emission slits were set to 2.5 nm for all the emission measurements. Steady state photoluminescence (PL) emission spectra of the synthesized HTMs were recorded on a JASCO F-8500 fluorescence spectrophotometer. Electrochemical responses of the synthesized anthracene based derivatives were exploited using the CH instrument model 680 Amp Booster with a standard three-electrode electrochemical cell consisting of glassy carbon as a working electrode, platinum wire as a counter electrode and Ag/AgCl as a reference electrode in acetonitrile containing 0.1 M tetrabutylammonium hexafluorophosphate as a supporting electrolyte at a scan rate of 100 mV s^{-1}. The Gaussian 09 program was used in quantum chemical calculations. The ground-state geometries were optimized by using the restricted B3LYP/6-31g (d, p) functions at the density functional theory (DFT) level.

Table 1 Energy level data of the designed HTMs

S. no.	HTMs	HOMO (eV)	LUMO (eV)	E_g (eV)
1	ANTTPA	−4.20	−1.71	2.48
2	AOME	−4.58	−1.90	2.68
3	AOHE	−4.54	−1.90	2.63

2.3. General procedure for the Heck coupling reaction (A)

4-(Bis(4-iodophenyl)amino)benzaldehyde (1 equiv.), vinylated aromatic compound (2 equiv.), Bu_4NBr (4 equiv.), and $Pd(OAc)_2$ (8 mol%) were dissolved in dry DMF/toluene (1 : 1) mixture. The resulting solution was purged under nitrogen for half an hour, then triethylamine (3 equiv.) was added as a base and the reaction mixture heated to 95 °C and maintained overnight. After completion of the reaction, the resulting mixture was passed through a Celite bed washed with ethyl acetate and water. The organic layer was further washed with a saturated brine solution and dried over anhydrous Na_2SO_4. The crude material was purified by column chromatography using petroleum ether/ethyl acetate as an eluent.

2.4. Synthesis of compound (4)

Compound **1** and compound **2** were synthesized according to previously reported literature.[21] Compound **3** was synthesized

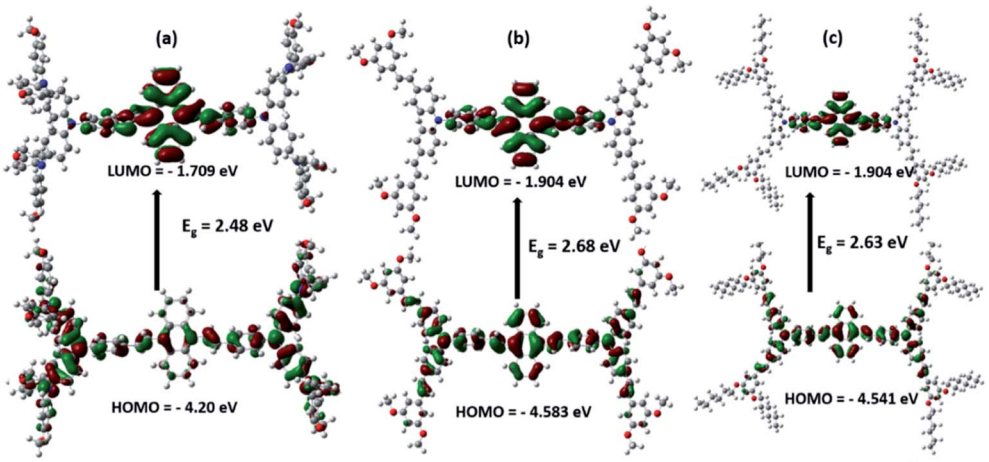

Fig. 3 Frontier orbitals of (a) ANTTPA, (b) AOME, (c) AOHE.

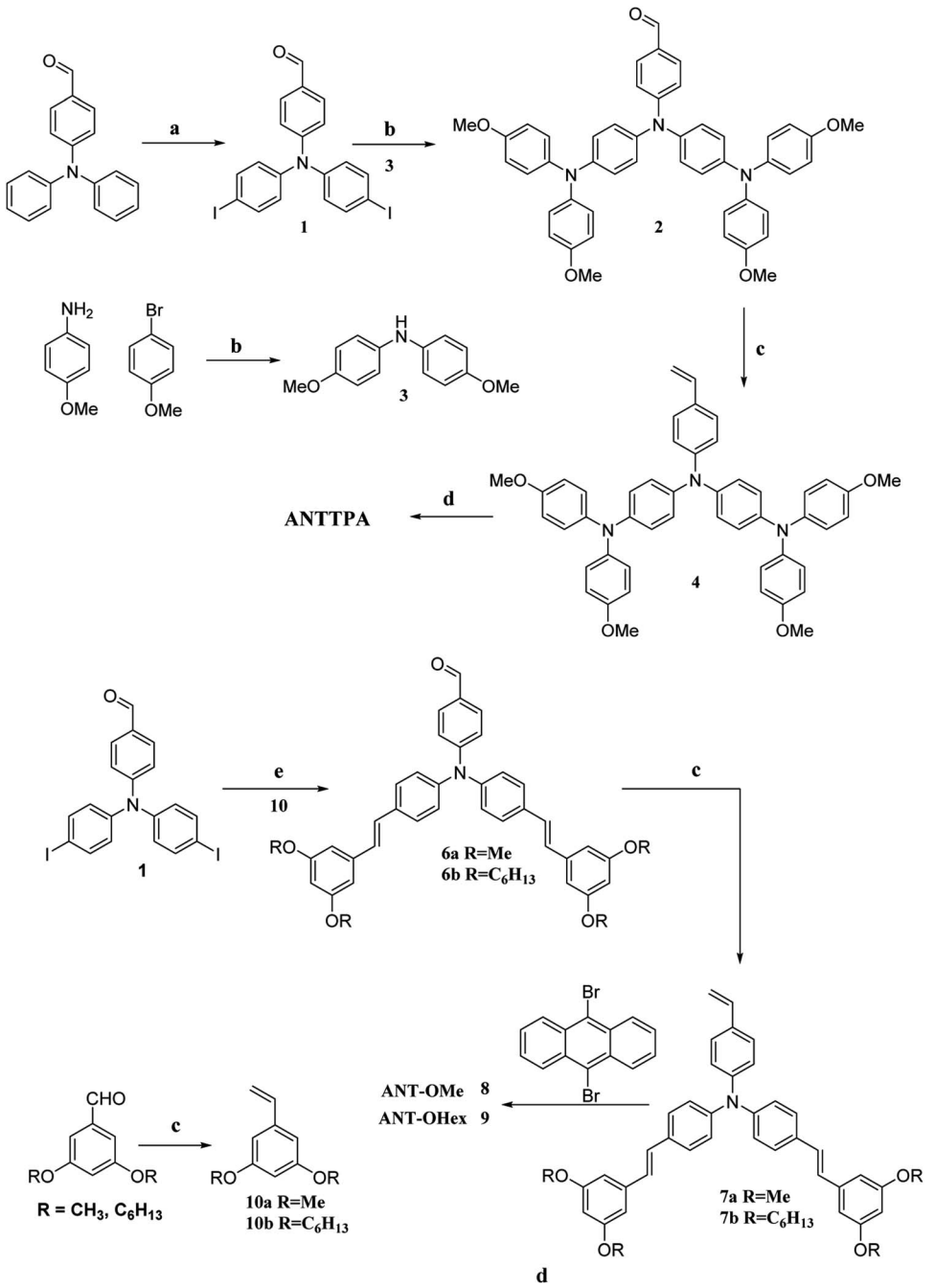

Scheme 1 Synthetic route of the designed HTMs ANTTPA, AOME, and AOHE. Reagent and conditions: (a) KIO_3/KI, CH_3COOH, 80 °C; (b) bis(tri-*tert*-butylphosphine)palladium(0), NaO*t*Bu, toluene, 95 °C, overnight; (c) methyltriphenylphosphonium iodide, DCM, KO*t*Bu, RT; (d and e) $Pd(OAc)_2$, tetrabutylammonium bromide, triethylamine, DMF/toluene (1 : 1), 95 °C.

by the same procedure as described for the synthesis of compound **2** except that compounds 1-bromo-4-methoxybenzene (2 g, 10.75 mmol) and 4-methoxyaniline (1.45 g, 11.8 mmol) were used.[22] To a stirred solution of compound **2**, 4-(bis(4-(bis(4-methoxyphenyl)amino) phenyl) amino)benzaldehyde (0.2 g, 0.482 mmol) and methyltriphenylphosphonium iodide (0.5 g, 1.272 mmol) were dissolved in DCM in a 100 mL round bottom flask, maintained under ice cold conditions. Furthermore, potassium *tert*-butoxide (0.2 g, 1.685 mmol) was portion wise added to the reaction mixture. The resultant solution was allowed to stir for 1 h, maintained under ice-cold conditions and then allowed to warm up to room temperature and stirred for about 5 h. After completion of the reaction, the reaction mixture was poured into water and then finally extracted with DCM twice, and the collected organic layer was washed with brine solution and dried over anhydrous Na_2SO_4. The solvent was evaporated under reduced pressure and the crude product was purified by column chromatography using petroleum ether/ethyl acetate (90 : 10), to afford a light greenish yellow solid, yield 65%. ^1H

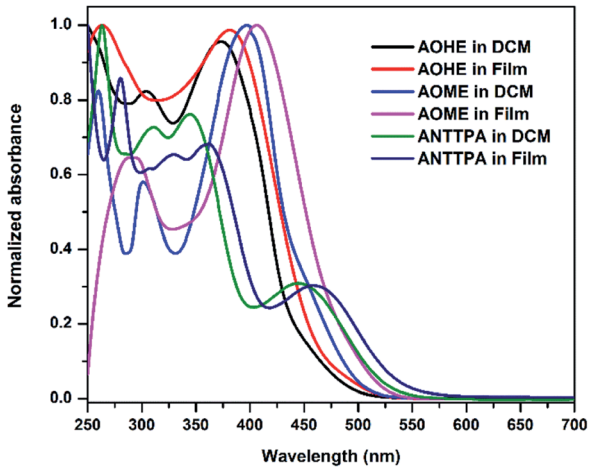

Fig. 4 Absorbance spectra of the synthesized HTMs in both solution and solid phase.

Table 2 Photophysical data of the synthesized HTM derivatives

	Solution (DCM)		Film	
HTMs	λ_{max} (nm)	λ_{emi} (nm)	λ_{max} (nm)	λ_{emi} (nm)
ANTTPA	444	606	463	617
AOME	397	567	407	575
AOHE	373	563	380	568

NMR (300 MHz, $CDCl_3$) δ 7.24 (d, J = 6 Hz, 2H), 7.04 (d, J = 9.0 Hz, 8H), 6.83 (d, J = 6 Hz, 2H), 6.81 (d, J = 8 Hz, 8H), 6.74 (d, J = 6.8 Hz, 8H), 6.62 (dd, J = 16 Hz, 1H), 5.59 (d, J = 16 Hz, 1H), 5.10 (d, J = 12 Hz, 1H) 3.78 (s, 12H).

2.5. Synthesis of compound *N*1,*N*1′-(((1*E*,1′*E*)-anthracene-9,10-diylbis(ethene-2,1-diyl))bis(4,1-phenylene))bis(*N*1-(4-(bis(4-methoxyphenyl)amino)phenyl)-*N*4,*N*4-bis(4-methoxyphenyl)benzene-1,4-diamine) (ANTTPA)

9,10-Dibromoanthracene (0.1 g, 0.342 mmol), compound **4** (0.5 g, 0.682 mmol), $Bu_4N^+Br^-$ (0.4 g, 1.2 mmol) and palladium(II) acetate (5 mol%) were dissolved in dry toluene/DMF (1 : 1). A 10 mL mixture was stirred and then the resultant solution was purged with nitrogen gas for about 30 minutes. Furthermore, triethylamine (0.190 mL, 1.03 mmol) was subsequently added to the reaction mixture and heated at 95 °C, and maintained overnight. After completion of the reaction by monitoring through TLC, the resultant mixture was passed through a Celite bed and washed with ethyl acetate. The organic layer was further washed with a saturated brine solution and dried over anhydrous Na_2SO_4. The crude product was purified by column chromatography silica gel, using chloroform/methanol (95 : 5), to afford a red orange solid, yield 60%. ^{1}H NMR (400 MHz, $CDCl_3$) δ 8.42 (d, J = 6.9 Hz, 4H), 7.78 (d, J = 16.4 Hz, 4H), 7.53 (d, J = 7.5 Hz, 4H), 7.46 (d, J = 7.3 Hz, 4H), 7.34 (d, J = 18.7 Hz, 4H), 7.08 (d, J = 8.5 Hz, 16H), 7.02 (d, J = 8.1 Hz, 8H), 6.91 (d, J = 8.6 Hz, 12H), 6.84 (d, J = 8.2 Hz, 12H), 3.80 (s, 24H). ^{13}C NMR (400 MHz, $CDCl_3$) δ 159.73, 145.69, 141.41, 134.03, 133.36, 132.21, 131.9, 131.22, 131.17, 130.80, 129.44, 128.62, 128.61, 128.58, 126.30, 114.72, 55.70. HR-MS m/z calcd. 1625.6976, found 1625.6964.

2.6. Synthesis of 4-((*E*)-3,5-dimethoxystyryl)-*N*-(4-((*E*)-3,5-dimethoxystyryl)phenyl)-*N*-(4-vinylphenyl)aniline (7a) and 4-((*E*)-3,5-bis(hexyloxy)styryl)-*N*-(4-((*E*)-3,5-bis(hexyloxy)styryl) phenyl)-*N*-(4-vinyl phenyl)aniline (7b)

Compounds **10a** and **10b** were synthesized as in previously reported literature.[23] Compounds **6a** and **6b** were synthesized according to general procedure **A** for Heck coupling.[24] Methyltriphenylphosphonium iodide (0.4 g, 1.00 mmol) and 4-(bis(4-((*E*)-3,5-dimethoxystyryl)phenyl)amino)benzaldehyde **6a** (0.5, 0.83 mmol) were dissolved in 10 mL of DCM under a nitrogen atmosphere and then KO*t*Bu (0.1 g, 1.67 mmol) was added portion wise slowly. The mixture was stirred for about 4 h. After completion of the reaction, the mixture was poured into 100 mL of water. The crude product was extracted with DCM and washed with brine. The combined organic layers were dried over anhydrous Na_2SO_4. The crude material was purified by column chromatography using petroleum ether/ethyl acetate (99 : 1) as an eluent, to afford a white solid as

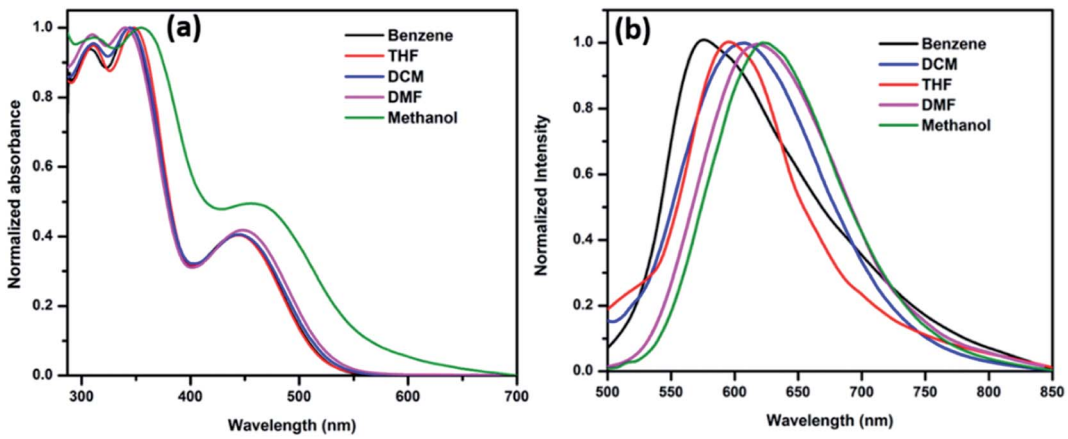

Fig. 5 (a) Normalized absorbance and (b) emission spectra of ANTTPA in various solvents.

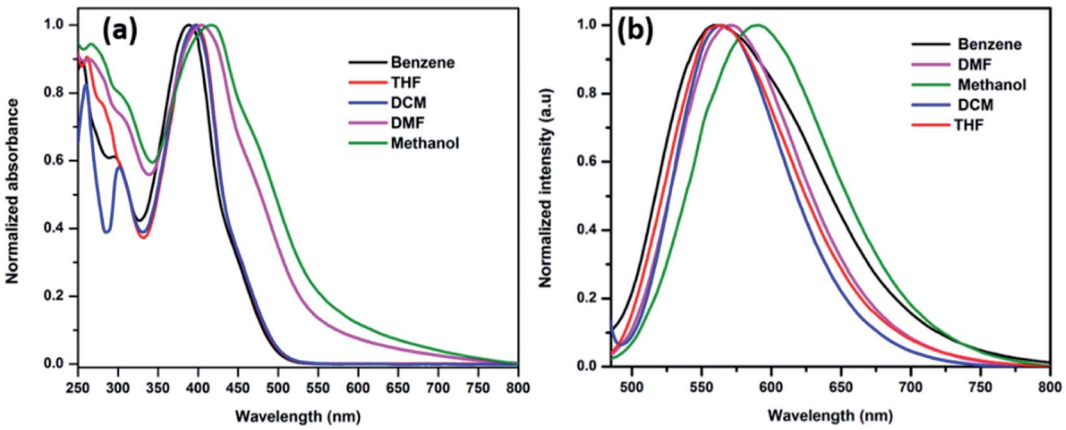

Fig. 6 (a) Normalized absorbance and (b) emission spectra of AOME in various solvents.

the product, yield 80%. ^{1}H NMR (300 MHz, $CDCl_3$) δ 7.41 (d, J = 8.5 Hz, 4H), 7.34 (d, J = 8.5 Hz, 2H), 7.10 (d, J = 8.3 Hz, 6H), 7.03 (s, 2H), 6.95 (d, J = 16.3 Hz, 2H), 6.67 (d, J = 2.0 Hz, 4H), 6.55–6.47 (m, 1H), 6.40 (s, 2H), 5.68 (d, J = 17.6 Hz, 1H), 5.20 (d, J = 10.9 Hz, 1H), 3.84 (s, 12H). ^{13}C NMR (75 MHz, $CDCl_3$) δ 161.44, 147.25, 147.22, 140.02, 136.57, 136.56, 133.09, 132.36, 129.00, 128.68, 127.68, 127.33, 124.73, 124.63, 112.97, 104.92, 100.26, 78.68, 78.19, 77.63, 77.00, 55.75. Compound **7b** was synthesized according to procedure for **7a**, using 4-(bis(4-((*E*)-3,5-dihexyloxystyryl)phenyl)amino)benzaldehyde (1 g, 1.28 mmol) **6b** and methyltriphenylphosphonium iodide (0.52 g, 1.28 mmol), KO*t*Bu (0.24 g, 2.14 mmol) to afford a light yellow viscous liquid, yield 78%. ^{1}H NMR (300 MHz, $CDCl_3$) δ 7.41 (d, J = 8.5 Hz, 4H), 7.34 (d, J = 8.5 Hz, 2H), 7.09 (d, J = 8.5 Hz, 6H), 7.03 (s, 2H), 6.97 (s, 2H), 6.66 (t, J = 4.6 Hz, 5H), 6.39 (s, 2H), 5.69 (d, J = 17.6 Hz, 1H), 5.20 (d, J = 11.0 Hz, 1H), 3.99 (t, J = 6.5 Hz, 8H), 1.86–1.74 (m, 8H), 1.48 (s, 8H), 1.43–1.25 (m, 17H), 0.94 (d, J = 6.7 Hz, 13H). ^{13}C NMR (75 MHz, $CDCl_3$) δ 160.89, 147.17, 139.79, 136.55, 132.95, 132.38, 128.72, 127.88, 127.60, 124.72, 112.94, 105.33, 101.06, 77.88, 77.45, 77.03, 68.47, 32.03, 29.70, 26.19, 23.05, 14.49.

2.7. Synthesis of 4,4′-((1*E*,1′*E*)-anthracene-9,10-diylbis(ethene-2,1-diyl))bis(*N*,*N*-bis(4-((*E*)-3,5-dimethoxystyryl)phenyl)aniline) (AOME)

9,10-Dibromoanthracene (0.1 g, 0.29 mmol), vinylated aromatic **7a** (0.35 g, 0.59 mmol), and $Bu_4N^+Br^-$(0.38 g, 1.19 mmol) were dissolved in dry DMF/toluene (1 : 1) mixture and then subsequently $Pd(OAc)_2$ (10 mg) added as a catalyst. The reaction mixture was purged under a nitrogen atmosphere for about 30 minutes, then triethylamine (0.09 g, 0.89 mmol) was added as a base and the mixture tightly capped and allowed to stir at 95 °C maintained overnight. After completion of the reaction, the resulting mixture was passed through the Celite bed and washed with ethyl acetate. The organic layer was further washed with a saturated brine solution and dried over anhydrous Na_2SO_4. The crude material was purified by column chromatography using petroleum ether/ethyl acetate (97 : 3) as an eluent, to afford a yellow solid as the product, yield 65%. ^{1}H NMR (300 MHz, $CDCl_3$) δ 8.42 (d, J = 3.2 Hz, 4H), 7.61 (d, J = 8.3 Hz, 4H), 7.46 (d, J = 8.6 Hz, 12H), 7.18 (d, J = 8.5 Hz, 12H), 7.04 (d, J = 15.7 Hz, 8H), 6.95 (d, J = 3.8 Hz, 4H), 6.69 (s, 8H), 6.41 (s, 4H), 3.85 (s, 24H). ^{13}C NMR (75 MHz, $CDCl_3$) δ 161.46, 147.48, 147.23, 140.01, 137.20,

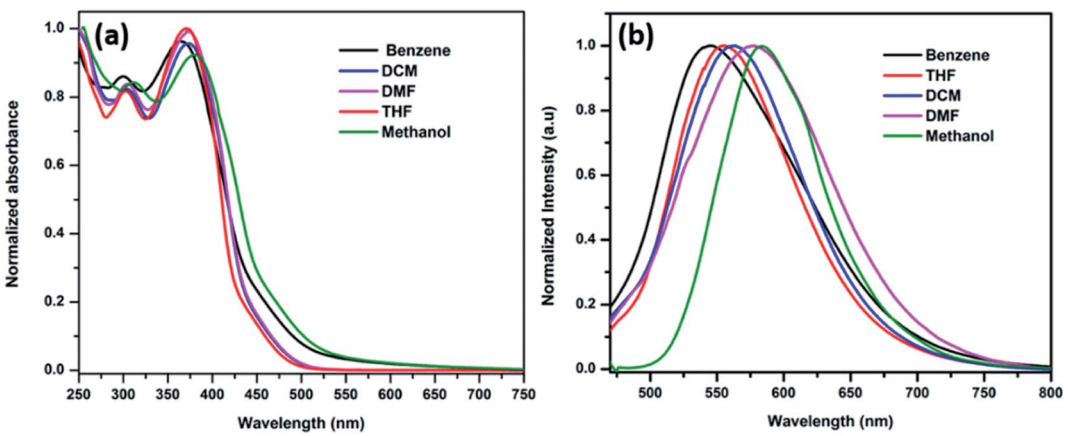

Fig. 7 (a) Normalized absorbance and (b) emission spectra of AOHE in various solvents.

Table 3 Photophysical data of the synthesized HTM derivatives

HTMs	Parameters	Benzene	THF	DCM	DMF	Methanol
ANTTPA	λ_{max} (nm)	443	445	444	450	453
	λ_{emi} (nm)	576	593	606	624	630
	Stokes shift (cm^{-1})	5210	5610	6020	6190	6200
AOME	λ_{max} (nm)	394	395	397	401	410
	λ_{emi} (nm)	560	562	567	576	595
	Stokes shift (cm^{-1})	7520	7530	7550	7557	7580
AOHE	λ_{max} (nm)	367	371	373	374	380
	λ_{emi} (nm)	545	556	563	578	590
	Stokes shift (cm^{-1})	8898	8960	9050	9310	9360

136.95, 133.14, 132.73, 130.08, 128.99, 128.24, 127.93, 127.03, 126.92, 125.59, 124.87, 124.69, 104.96, 100.28, 55.77. HRMS *m*/*z* calcd. 1365.5948, found 1365.5954.

2.8. Synthesis of 4,4′-((1*E*,1′*E*)-anthracene-9,10-diylbis(ethene-2,1-diyl))bis(*N*,*N*-bis(4-((*E*)-3,5-bis(hexyloxy) styryl)phenyl)aniline) (AOHE)

Compound **9** was synthesized according to the procedure for AOME using 9,10-dibromoanthracene (0.1 g, 0.30 mmol), vinylated aromatic **7b** (0.55 g, 0.61 mmol), tetra-butylammonium bromide (0.38 g, 1.19 mmol), and triethylamine (0.09 g, 0.892 mmol) to afford a red colored solid, yield 60%. ^{1}H NMR (300 MHz, $CDCl_3$) δ 8.37 (d, J = 3.2 Hz, 4H), 7.53 (d, J = 8.4 Hz, 4H), 7.37 (d, J = 8.4 Hz, 12H), 7.10 (d, J = 8.3 Hz, 12H), 6.95 (d, J = 17.5 Hz, 12H), 6.60 (s, 8H), 6.32 (s, 4H), 3.91 (t, J = 6.3 Hz, 16H), 1.72 (dd, J = 14.0, 6.7 Hz, 18H), 1.52–1.19 (m, 44H), 0.86 (q, 26H). ^{13}C NMR (75 MHz, $CDCl_3$) δ 160.97, 147.51, 147.17, 139.84, 137.21, 133.16, 132.67, 130.09, 128.76, 127.98, 126.97, 126.54, 125.59, 124.71, 105.50, 101.28, 68.54, 32.02, 29.72, 26.18, 23.02, 14.43. HRMS *m*/*z* calcd. 1926.2208, found 1926.2202.

3. Results and discussion

3.1. Theoretical investigation

The ground state, excited state and band gap energy level play a crucial role in the perovskite solar cells. The energy level alignments of our designed materials were theoretically investigated by a Gaussian 09 program. The optimized structure (Fig. 2) and density of electron were determined by using quantum chemical calculation at the B3LYP/6-31g (d, p) basis set level. The electrons in the ground state are distributed throughout the molecule, but when the molecule is in the excited state, the electron density is localized in the center core of the anthracene unit, which indicates an intramolecular charge transfer (ICT) between the substituted triphenylamine and anthracene (Fig. 3). The HOMO energy level of our designed HTMs is higher compared to that of perovskite, so that a hole is easily generated; at the same time, the HOMO energy level of HTM is lower when compared to that of the counter electrode. Our designed materials fulfilled the interface energy levels (TiO_2/perovskite/HTM/counter electrode). Furthermore, our designed materials have enough LUMO energy to increase the charge recombination resistance processes. In addition to that, the HOMO energy levels of the AOME and AOHE compounds are closer to the perovskite HOMO energy level compared to that of the ANTTPA. This closer energy relationship is present due to the increasing conjugation in the AOME and AOHE materials. All the characteristic data are tabulated in Table 1.

3.2. Synthetic strategy and characterization of the HTMs

The chemical structure of the newly designed D–π–D–π–D and $(D–\pi)_2$–D–$(\pi–D)_2$ short and long alkyl substituted triphenylamine and anthracene based HTMs are ATNTPA, AOME, and AOHE and their synthetic routes are shown in Scheme 1. Initially, the core of the dibromo anthracene was synthesized by a bromination reaction, and further, a Vilsmeier–Haack reaction was carried out for the synthesis of the triphenylamine mono aldehyde, then the triphenylamine mono aldehyde was reacted with potassium iodide and iodate in acetic acid to form the diiodo mono aldehyde of the triphenylamine derivative, and in the meantime short and long alkyl substituted donors were synthesized by stepwise reactions, which were reacted with the diiodo substituted triphenylamine mono aldehyde derivatives through Buchwald–Hartwig and Mizoroki–Heck cross coupling reactions. These cross coupled derivatives were reacted with the

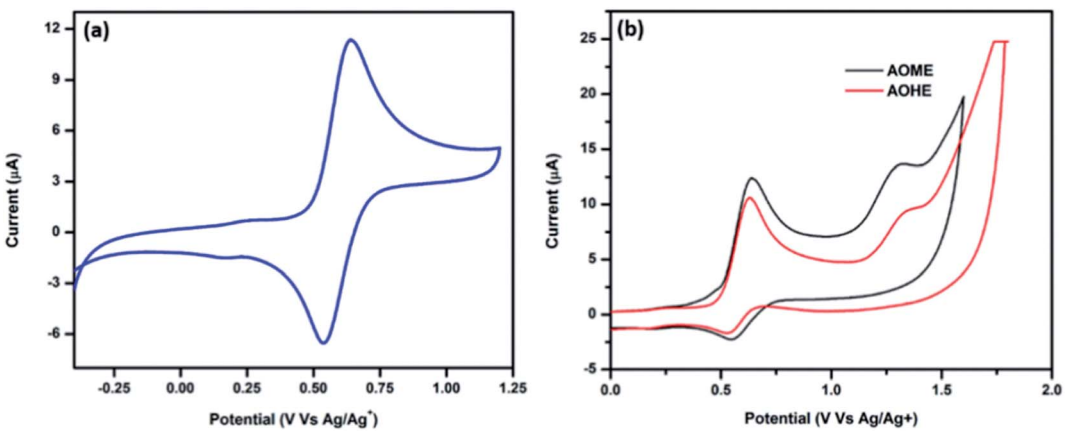

Fig. 8 Cyclic voltammogram of (a) ANTTPA (b) AOME and AOHE in DCM solvent at a scan rate of 100 mV s^{-1}.

Table 4 Electrochemical properties and energy level properties of ANTTPA, AOME and AOHE

HTMs	$E^{onset a}$ (V)	$E_p^{oxi\ b}$ (V)	HOMO^c (eV)	LUMO^c (eV)	$E_g{}^d$ (eV)	HOMO^e (eV)	LUMO^e (eV)	$E_g{}^e$ (eV)
ANTTPA	0.39	0.64	−5.15	−3.02	2.13	−4.20	−1.71	2.48
AOME	0.33	0.65, 1.31	−5.09	−2.81	2.28	−4.58	−1.90	2.68
AOHE	0.46	0.63, 1.29	−5.22	−2.79	2.43	−4.54	−1.90	2.63

[a] Onset oxidation potential. [b] Peak potential. [c] Experimentally calculated. [d] Experimentally calculated from UV-Vis spectra. [e] Theoretically calculated using DFT.

core material of dibromo anthracene by a Mizoroki–Heck coupling reaction to obtain the two molecular architectures, D–π–D–π–D and $(D–π)_2$–D–$(π–D)_2$. Column chromatography was used to purify the synthesized HTMs. Hereafter, the synthesized HTMs were confirmed by ^{1}H, ^{13}C NMR, and HR-MS. Furthermore, the synthesized HTMs were studied by their photophysical, morphological, and electrochemical properties.

3.3. Optical properties of the HTMs

The photophysical properties of the synthesized HTMs ANTTPA, AOME, and AOHE were studied in both UV-visible absorbance and emission spectroscopy, and were recorded in two phases, such as in solution and the film phase (solid) (Fig. 4). The UV-visible absorbance of ANTTPA shows three absorbance bands, the higher energy absorbance may be attributed to n–π* transition, the low energy absorbance band is due to the intramolecular charge transfer (ICT) and the emission band of ANTTPA is 606 nm, so the 606 nm band is due to the ICT. AOME and AOHE absorbance bands at 397 and 373 nm may be attributed to the ICT between the triphenylamine and center core of the anthracene, and emission bands are 567 and 563 nm are observed, respectively. The characteristic data are given in Table 2. The maximum absorbance and emission bands of ANTTPA were bathochromically shifted compared to AOME and AOHE. This bathochromic shift is due to the twisted structure of ANTTPA compared to those of AOME and AOHE. The twisted structure of ANTTPA was examined by DFT studies through a dihedral angle.[25,26] Our molecule has a C_{2V} symmetry in nature, so we modified the HTMs in two factors, such as an olefin bond insertion between the triphenylamine and 1,3-dimethoxybenzene substituted (AOME) or 1,3-bis(hexyloxy)benzene substituted (AOHE), and another HTM has no olefin bond insertion between the donor (triphenylamine) and the donor (bis(4-methoxyphenyl)amine substituted). The dihedral angles of triphenylamine in the ANTTPA, AOME, and AOHE are 145.5°, 140.3°, and 137.2°, respectively (Fig. S8–S10†). Among these HTMs, ANTTPA has the highest dihedral angle compared to those the AOME and AOHE, and hence ANTTPA has a more twisted structure compared to those of AOME, AOHE.

The ICT band was further investigated using solvatochromism experiments, which is based on the solvent polarity from non-polar to polar solvents. The influence of solvents in synthesized HTMs were determined by both absorbance and emission spectroscopy. The ANTTPA (Fig. 5a), AOME (Fig. 6a) and AOHE (Fig. 7a) UV-visible absorbance spectra have a slightly bathochromic shift from non-polar to polar solvents. The emission band is found to shift towards longer wavelengths with increasing solvent polarity, and this the shift is due to the stabilization of the charge-transfer transition in polar solvents (Fig. 5b, 6b, and 7b). A Dimroth–Reichardt solvent polarity correlations plot of ANTTPA, AOME and AOHE (Fig. S11–S13†) shows higher values of Stokes shift on moving from non-polar to polar solvents, which suggests that the intramolecular charge transfer transition is higher when compared to that of the ground state.[27,28] All the characteristic data are tabulated in Table 3. The DFT studies also prove that in the ground state of synthesized HTMs, electrons are located in the terminal donor group, but in the excited state electrons are delocalized in the center core of the anthracene, which may be due to the ICT between the terminal donor to the center core of the anthracene.

3.4. Electrochemical properties

The electrochemical properties of all of the anthracene-based compounds were studied in DCM solvent using cyclic voltammetry (CV) with tetrabutylammonium hexafluorophosphate ($TBAPF_6$) as the supporting electrolyte and ferrocene as the internal reference. The usual three electrode setup consisted of a platinum wire counter electrode, glassy carbon working electrode, and Ag/AgCl reference electrode at a scan rate of 100 mV s^{-1}. The ANTTPA compound has quasi reversible redox peaks, as shown in Fig. 8a. The oxidation peak potential of ANTTPA at 0.64 V is due to a radical cation formation attributed to the removal of an electron from the triphenylamine moiety. The

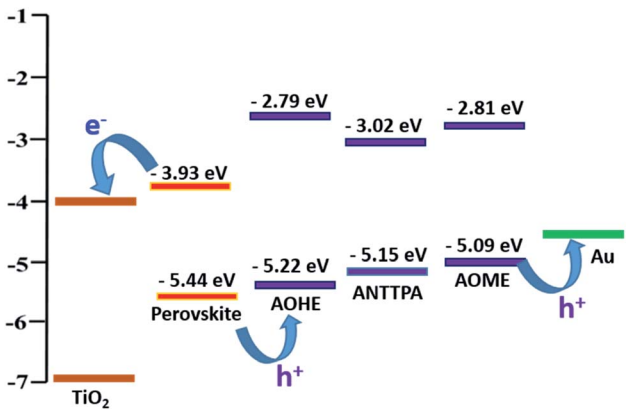

Fig. 9 Energy levels of the anthracene based HTMs and their alignment with the perovskite.

AOME and AOHE have a two peak oxidation potential and a one reduction peak potential. The first oxidation peak potential of AOME is 0.65 V and the second oxidation peak potential is 1.31 V, representing the formation of stable cation and dications (Fig. 8b). The AOHE has two oxidation peak potentials at 0.63 and 1.29 V, respectively; this peak potential represents the formation of stable cation and dications. The ground state to excited state is determined by the onset oxidation potential in the DCM solution. The optical band gap energy is calculated from the onset absorbance band in the film phases by using this equation $E_g = 1243/\lambda_{onset}$. The onset oxidation potentials of ANTTPA, AOME and AOHE are 0.39, 0.33, and 0.46 V, respectively, these onset values are substituted in the equation HOMO $= -e(E^{onset} + 4.76)$ and finally the HOMO energy level of the synthesized compounds obtained. The LUMO energy levels are determined from this equation LUMO = HOMO $- E_g$. All of the energy levels are tabulated in Table 4.

The HOMO energy levels of our HTMs are shown in Fig. 9. From the figure, we observe that our HTMs have a lower HOMO energy level than the HOMO energy level of spiro-OMeTAD (-5.02 eV)[12] and well match the perovskite (-5.44 eV) energy level. These energy levels are sufficient to generate the holes from the perovskite layer to the hole transporting layer, when the perovskite layer is absorbed by sunlight. In our synthesized HTMs, the LUMO energy level is nearly -2.79 to -3.02 eV, LUMO energy levels that are suppressed by the charge recombination process. Furthermore, the hexyl substituted and more conjugated $(D–\pi)_2–D–(\pi–D)_2$ architecture of AOHE has a closer HOMO energy level to the perovskite HOMO energy level when compared to the ANTTPA and AOME levels. Finally, the calculated energy levels of the synthesized anthracene-based compounds have the potential to be applied as hole transporting materials in the hybrid perovskite solar cells.

3.5. Solubility and stability of the synthesized HTMs

In the device fabrication, chlorobenzene solvent is a reference solvent for dissolving the HTMs. Consequently, we measured their solubility values in chlorobenzene, and we found that 70–75 mg of spiro-OMeTAD, 80–86 mg of ANTTPA, 92–98 mg of AOME, and 120 mg of AOHE can be dissolved in 1 mL of chlorobenzene at room temperature. The surface morphology of the pristine perovskite film and the synthesized HTM coated on the perovskite film was inspected by scanning electron microscope (SEM) images. Fig. 10a shows that the pristine perovskite film has a regularly ordered morphological structure, a similar morphology to that observed by P. Y. Su *et al.*[29] Furthermore, our synthesized HTMs and spiro-OMeTAD were coated on top of the perovskite film. When the spin coating was carried out with spiro-OMeTAD, the perovskite layer is partially covered, but our synthesized HTMs show a uniform film on top of the perovskite layer (Fig. 10c–e). Among these HTMs, AOHE shows a highly homogeneous film formation on the top of the perovskite layer.[30] Therefore, the results illustrate that the insertion of an olefin bond increases the solubility and good film forming capability, and moreover AOHE has a highly soluble and highly homogeneous film due to the presence of a hexyl group in the HTM which suppresses the intermolecular aggregation of AOHE. The absolute hardness (η) helps to determine the stability of the organic material to a certain extent. The absolute hardness η can be calculated by the equation $\eta = (IP - EA)/2$, where IP is the adiabatic ionization potential and EA the adiabatic electron affinity. The calculated η values of ANTTPA, AOME, AOHE, and spiro-OMeTAD are 1.06, 1.14, 1.22, and 1.46 eV, respectively. The lower absolute hardness η values indicate that the material has

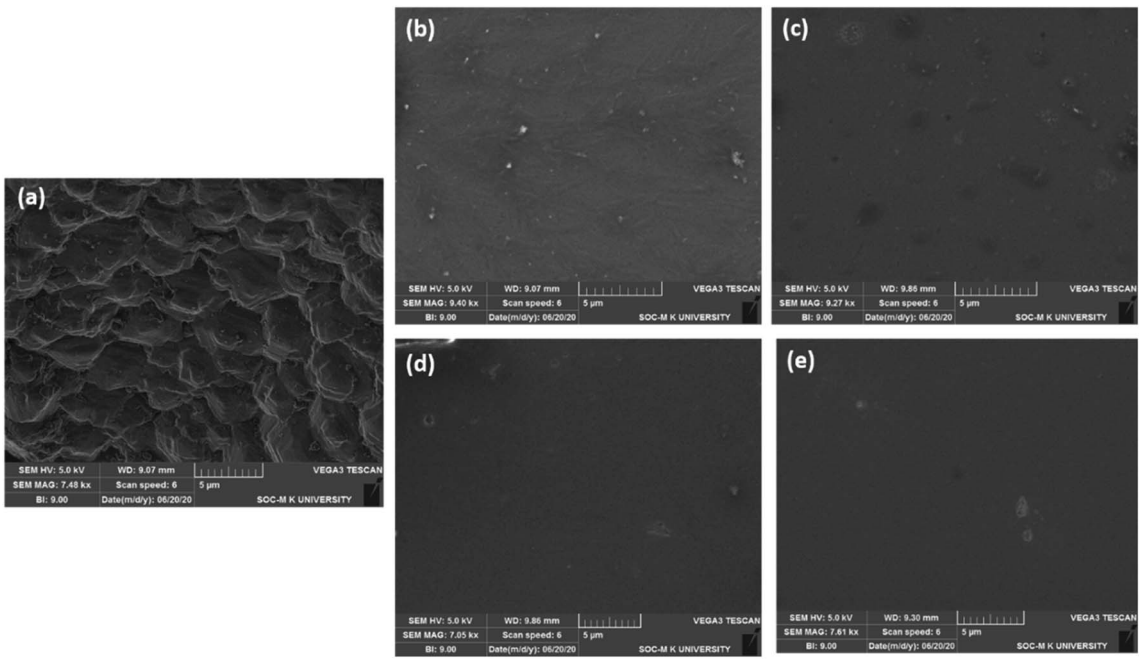

Fig. 10 SEM images of the (a) pristine perovskite film, (b) spiro-OMeTAD, (c) ANTTPA, (d) AOME, and (e) AOHE spin coated on the perovskite film.

a better stability,[31,32] so that our synthesized materials have a high stability compared to that of the spiro-OMeTAD.

4. Conclusion

In summary, we report two novel star shaped D–π–D–π–D and $(D–\pi)_2–D–(\pi–D)_2$ anthracene based HTMs, ANTTPA, AOME, and AOHE. Firstly, we measured the band gap of the materials using in the Gaussian 09 program and our designed compound energy levels are suitable for their use as HTMs in solar cell devices. After that, our designed materials were synthesized from Buchwald–Hartwig and Mizoroki–Heck cross coupling reactions with a high yield of products. The synthesized materials were confirmed by ^{1}H NMR, ^{13}C NMR and HR-MS techniques. The optical properties of the novel synthesized star-like compounds of ANTTPA, AOME, and AOHE were carried out in various polar and non-polar solvents. All the derivatives have a bathochromic shift with an increase in solvent polarity. These studies clearly show that charge transporting behavior present in our synthesized compounds. The HOMO energy level of AOHE is very closer to the HOMO energy level of the perovskite, and this closer energy may be due to the long alkyl chain present in AOHE compound. The observed theoretical studies, optical properties, electrochemical studies, solubility and stability studies highlight that the anthracene-based compounds are potential candidates for use as HTMs in organic–inorganic hybrid perovskite solar cells.

Conflicts of interest

There are no conflicts to declare.

Acknowledgements

We acknowledge financial support from the Council of Scientific and Industrial Research (CSIR), HRDG, File No. 01(2901)/17/EMR-II, New Delhi and the Department of Science and Technology, SERB, the Extramural Major Research Project (Grant No. EMR/2015/000969), the Department of Science and Technology DST/TM/CERI/C130(G), New Delhi, India. Further, we also acknowledge the DST-FIST, DST-IRPHA, DST-PURSE, UGC-UPE and UGC-NRCBS, SBS, MKU for providing instrumental facilities.

References

1 A. Kojima, K. Teshima, Y. Shirai and T. Miyasaka, *J. Am. Chem. Soc.*, 2009, **131**, 6050.
2 J. Liu, Y. Wu, C. Qin, X. Yang, T. Yasuda, A. Islam, K. Zhang, W. Peng, W. Chen and L. Han, *Energy Environ. Sci.*, 2014, **7**, 2963.
3 W. Chen, Y. Wu, Y. Yue, J. Liu, W. Zhang, X. Yang, H. Chen, E. Bi, I. Ashraful, M. Gratzel and L. Han, *Science*, 2015, **350**, 944.
4 M. Saliba, T. Matsui, K. Domanski, J.-Y. Seo, A. Ummadisingu, S. M. Zakeeruddin, J.-P. Correa-Baena, W. R. Tress, A. Abate, A. Hagfeldt and M. Gratzel, *Science*, 2016, **354**, 206.
5 K. T. Cho, S. Paek, G. Grancini, C. Roldan-Carmona, P. Gao, Y. Lee and M. K. Nazeeruddin, *Energy Environ. Sci.*, 2017, **10**, 621.
6 B. Cai, Y. Xing, Z. Yang, W.-H. Zhang and J. Qiu, *Energy Environ. Sci.*, 2013, **6**, 1480.
7 Y. S. Kwon, J. Lim, H.-J. Yun, Y.-H. Kim and T. Park, *Energy Environ. Sci.*, 2014, **7**, 1454.
8 L. Zhu, Y. Shan, R. Wang, D. Liu, C. Zhong, Q. Song and F. Wu, *Chem.–Eur. J.*, 2017, **23**, 4373.
9 C. Huang, W. Fu, C.-Z. Li, Z. Zhang, W. Qiu, M. Shi, P. Heremans, A. K. Y. Jen and H. Chen, *J. Am. Chem. Soc.*, 2016, **138**, 2528.
10 I. Garcia-Benito, I. Zimmermann, J. Urieta-Mora, J. Aragó, A. Molina- Ontoria, E. Orti, N. Martin and M. K. Nazeeruddin, *J. Mater. Chem. A*, 2017, **5**, 8317.
11 H. Li, K. Fu, A. Hagfeldt, M. Grätzel, S. G. Mhaisalkar and A. C. Grimsdale, *Angew. Chem.*, 2014, **53**, 4085.
12 R. Grisorio, B. Roose, S. Colella, A. Listorti and G. P. Suranna, *ACS Energy Lett.*, 2017, **2**, 1029.
13 S. Carli, J. P. Baena, G. Marianetti, N. Marchetti, M. Lessi, A. Abate, S. Caramori, M. Grätzel, F. Bellina and C. A. Bignozzi, *ChemSusChem*, 2016, **9**, 657.
14 A. Abate, S. Paek, F. Giordano, J. P. Correa-Baena, M. Saliba, P. Gao, T. Matsui, J. Ko, S. M. Zakeeruddin and K. H. Dahmen, *Energy Environ. Sci.*, 2015, **8**, 2946.
15 H. Choi, H. Jo, S. Paek, K. Ko, H. M. Ko, J. K. Lee and J. Ko, *Chem.–Asian J.*, 2015, **11**, 548.
16 A. Krishna, D. Sabba, J. Yin, A. Bruno, P. P. Boix, Y. Gao, H. A. Dewi, G. G. Gurzadyan, C. Soci and S. G. Mhaisalkar, *Chem.–Eur. J.*, 2015, **21**, 15113.
17 F. Zhang, Z. Wang, H. Zhu, N. Pellet, J. Luo, C. Yi, X. Liu, H. Liu, S. Wang, X. Li, Y. Xiao, S. M. Zakeeruddin, D. Bib and M. Grätzel, Over 20% PCE perovskite solar cells with superior stability achieved by novel and low-cost hole-transporting materials, *Nano Energy*, 2017, **41**, 469.
18 A. Marrocchi, F. Silvestri, M. Seri, A. Facchetti, A. Taticchi and T. J. Marks, *Chem. Commun.*, 2009, 1380.
19 J. Huang, J. H. Su and H. Tian, *J. Mater. Chem.*, 2012, **22**, 10977.
20 H. Meng, F. Sun, M. B. Goldfinger, F. Gao, D. J. Londono, W. J. Marshal, G. S. Blackman, K. D. Dobbs and D. E. Keys, *J. Am. Chem. Soc.*, 2006, **128**, 9304.
21 R. Balasaravanan, V. Sadhasivam, A. Siva, M. Pandi, G. Thanasekaran and C. Arulvasu, *ChemistrySelect*, 2016, **1**, 2792.
22 R. Balasaravanan, V. Sadhasivam, G. Sivaraman and A. Siva, *Asian J. Org. Chem.*, 2016, **5**, 399.
23 R. Balasaravanan and A. Siva, *New J. Chem.*, 2016, **40**, 5099.
24 M. Harikrishnan, V. Sadhasivam, A. Siva, S. Anandan, V. Subbiah and S. Murugesan, *J. Phys. Chem. C*, 2019, **123**, 21959.
25 J. Tagare, H. Ulla, M. N. Satyanarayan and S. Vaidyanathan, Synthesis, photophysical and electroluminescence studies of new triphenylamine-phenanthroimidazole based materials for organic light emitting diodes, *J. Lumin.*, 2018, **194**, 600.

26 H. Choi, K. Do, S. Park, J. S. Yu and J. Ko, Efficient Hole Transporting Materials with Two or Four *N,N*-Di(4-methoxyphenyl)aminophenyl Arms on an Ethene Unit for Perovskite Solar Cells, *Chem.–Eur. J.*, 2015, **21**, 15919.

27 R. Balasaravanan, K. Duraimurugan, J. Sivamani, V. Thiagarajan and A. Siva, Synthesis and photophysical properties of triphenylamine-based multiply conjugated star-like molecules, *New J. Chem.*, 2015, **39**, 7472.

28 M. Harikrishnan, V. Sadhasivam, M. Mariyappan, S. Murugesan, N. Malini and A. Siva, A simple triazine (D–A) based organic fluorophore selective dual sensor for Copper(II) and dichromate ions and its solvatochromism, solid state sensing, logic gate applications, *Dyes Pigm.*, 2019, **168**, 123.

29 P. Y. Su, L. B. Huang, J. M. Liu, Y. F. Chen, L. M. Xia, D. B. Kuang, M. Mayor and C. Y. Su, A multifunctional poly-*N*-vinylcarbazole interlayer in perovskite solar cells for high stability and efficiency: a test with new triazatruxene-based hole transporting materials, *J. Mater. Chem. A*, 2017, **5**, 1913.

30 L. Zhu, Y. Shan, R. Wang, D. Liu, C. Zhong, Q. Song and F. Wu, High-Efficiency Perovskite Solar Cells Based on New TPE Compounds as Hole Transport Materials: The Role of 2,7- and 3,6- Substituted Carbazole Derivatives, *Chem.–Eur. J.*, 2017, **23**, 4373.

31 W. J. Chi, Q. S. Li and Z. S. Li, Exploring the electrochemical properties of hole transport materials with spiro-cores for efficient perovskite solar cells from first-principles, *Nanoscale*, 2016, **8**, 6146.

32 H. Liu and X. Liu, Strategy to modulate the π-bridged units in bis(4-methoxyphenyl)amine-based hole-transporting materials for improvement of perovskite solar cell performance, *J. Mater. Chem. C*, 2018, **6**, 6816.

